# Finite Element Simulation of Shear Wave Propagation Induced by a VCTE Probe

S.Audière[*,1,2], E.Angelini[1], M.Charbit[1], V.Miette[2], J.Oudry[2] and L.Sandrin[2]
[1]Institut Telecom, Telecom ParisTech, [2]Echosens, Research Department
*46 Rue Barrault, 75013 Paris, stephane.audiere@telecom-paristech.fr

**Abstract:** The Fibroscan® (Echosens, Paris, France) device based on vibration–controlled transient elastography (VCTE) is used to non–invasively assess liver stiffness correlated to the hepatic fibrosis. Stiffness is quantified by measuring the velocity of a low–frequency shear wave traveling through the liver, which is proportional to the Young's modulus E. It has been demonstrated that E is highly correlated with liver fibrosis stage as assessed by liver biopsy. To study the emergence of a two shear wave with different velocity in liver detected with the Fibroscan® on different in vivo cases, simulations with finite element models (FEM) on a 3D anatomical model of liver and ribs can help to understand this propagation patterns. Indeed, the shape and the direction of the shear wave front induced by the Fibroscan® probe in the liver are not entirely known.

**Keywords:** elastography, shear wave, VCTE, Fibroscan, liver.

## 1. Introduction

Elastography is a branch of tissue characterization which encompasses a large panel of techniques used to measure or describe the elastic properties of tissues. In the following we are only concerned with the stiffness which is defined by the Young's modulus (expressed in Pascal).

Elastographic techniques can be categorized into three groups depending on the way to generate a mechanical excitation of the tissues. In static elastography [1], developed by Ophir *et al.*, the tissues are insonified before and after a small compression and the speckle distortion due to the compression is related to the stiffness of the medium. A second set of applications use the deformations generated in the tissues by the natural movements of the organs [2], [3]. Finally, dynamic elastography relies on the study of the propagation of low frequency shear waves generated either monochromatically in the case of magnetic resonance elastography (MRE) [4] and sonoelastography ([5]) or transiently in the case of transient elastography [7-9]. The impulse excitation used in transient elastography is generated either by an external vibrator or by a transient ultrasound radiation force [6], [7].

*In vivo* measurements were obtained using these different elastographic techniques on a variety of organs such as breast, prostate [8]. Fibroscan® (Echosens, Paris, France) is used to assess liver fibrosis by measuring liver stiffness. Fibroscan® is a parametric, transient elastography based technique which provides an average value of the Young's modulus in a region of interest comprised between 25 and 65 mm below the skin. This device is non-invasive, fully automatic and gives a result within a few minutes. Its main advantages are its ease of use, its good reproducibility and a very good acceptance by patients. Clinical interest of liver stiffness measurement using Fibroscan® has been largely validated for adult patients with chronic liver diseases [9]. About 900 devices sold throughout the world, mainly in Europe and Asia. Echosens has over 300 peer-reviewed clinical publications to its credit.

## 2. Method & Material

Liver elasticity measured by Fibroscan® ranges between 2–75kPa and corresponds to a shear wave velocity range of 0.8–5 m/s. The shear wave is mechanically induced by the displacement of a piston controlled with an apodized 20 ms period sinusoidal impulse (see Figures 1 & 2).

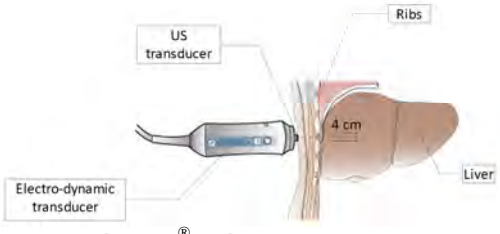


**Figure 1**. Fibroscan® Probe.

The movements of tissues are observed in time using an ultrafast ultrasound scanner (3.5 MHz) with a pulse repetition frequency of 6000Hz. Inter-correlation method between successive RF

lines provides the strain image in the plane where the horizontal axis represents the time and the vertical one the depth. Figure 3, we have reported the amplitude of the strain in grayscale. We observe the shear wave.

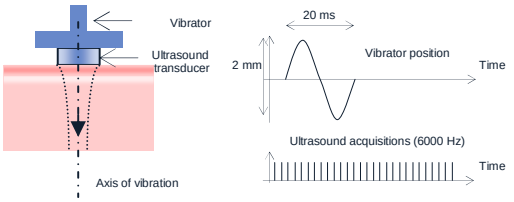


**Figure 2**. Acquisition.

From the slope of the negative wavefront, we estimated the shear wave velocity and we then deduced the Young's modulus using the following formula

$$E = 3\rho V_S^2 \qquad (1)$$

where $\rho$ is the medium density and *Vs* the shear wave velocity.

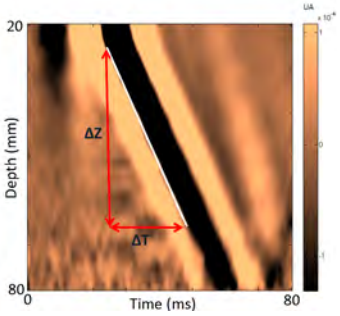


**Figure 3**. Elastogram or Strain Image.

This work used the Structural Mechanics Module available in COMSOL Multiphysics to develop computational models for the previously presented experiment.

In the first simulation we have verified the goodness of fit between the computational model and the analytical one. That shown that, in this case, a good spatio-temporal grid of computation may be reached.

In the second simulation, we have verified the goodness of fit with a true experiment on a phantom which mimics homogeneous tissues (see Figure 4). That is important for us because our goal is to dispose of a virtual experiment. We also expect that these results may highlight the uncertainty of measurement, noise due to the observation device.

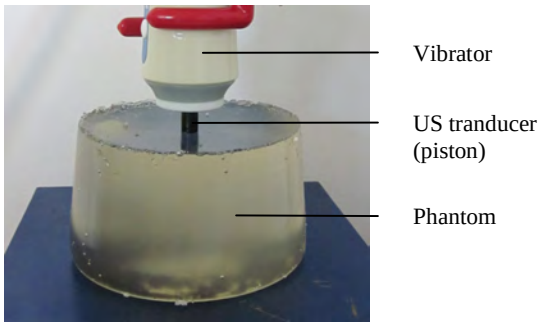


**Figure 4**. Photography experience

The last simulation consisted, with a 3D model, of generating the shear wave and the propagation induced by a piston hitting the phantom or the liver. The liver surface mesh has been created and distributed by the IRCAD (Strasbourg, France [10]).

## 3. Theoretical aspects

In this section, we present briefly the analytical expression of the response at an impulsive stress of a linear, isotropic, purely elastic, semi-infinite and quasi-incompressible medium.

In [11], the authors yielded the analytical solution of the problem based on the elastodynamic Green's functions. These functions are decomposed into a term of compression, a shear term and a coupling term. The latter term has been often neglected. It has been studied by Sandrin et al. [12] for a non punctual stress. They gave the following analytical expression of the media Green's function, in the case of a cylindrical piston[1]:

$$g(z,t) = \begin{cases} \dfrac{R^2 t}{\rho(z^2+R^2)^{3/2}} & if \quad 0 \le t \le \dfrac{\sqrt{z^2+R^2}}{V_S} \\ 0 & if \quad \dfrac{\sqrt{z^2+R^2}}{V_S} \le t \end{cases} \qquad (2)$$

where $R$ is the radius of the piston, $z$ and $t$ respectively the depth and the time. The Green's function $g$ takes into account both diffraction and coupling effects for circular sources on homogeneous and isotropic half-space media.

[1] Equation (10) corresponds to the equation (36) of reference [11], where we have omitted the term *a* which is given by the expression (3).

The stress, induced by the piston and expressed in Pascal, writes

$$a(t) \propto \frac{d^2 m_p(t)}{dt^2} \tag{3}$$

where $m_p(t)$ denotes the displacement of the piston. Because the different assumptions, the displacement field reduced to only one non-null component along z-axis. The expression is given by

$$u_{zz}(z,t) \propto \int g(t-\theta,z)a(\theta)d\theta \propto \frac{1}{(z^2+R^2)^{3/2}} \int_0^T \frac{d^2 m_p}{du^2}(t-u)udu \tag{4}$$

where $T = \sqrt{R^2+z^2}/V_S$.

After few calculations, we had

$$\varepsilon_{zz}(z,t) \propto \frac{z}{(z^2+R^2)^{5/2}}\left(m_p(t) - m_p(t-T) - T\dot{m}_p(t-T)\right) \tag{5}$$

where $\dot{m}_p$ denotes the first derivative.

## 4. Use of COMSOL Multiphysics

### 4.1. Validation model

For the model validation (comparison with analytical and experimental results) is used an axisymmetric model. The Young's modulus given by measurement of three identical phantoms elasticity is 6 kPa. The Poisson's ratio is fixed at 0.4999, that corresponds to an incompressive medium. Equation 1, with $\rho$ = 1kg/L, implies a shear wave velocity propagation of 1.41 m.s$^{-1}$. The maximum size of the finite element mesh is 1 mm for a total of 17669 meshes. This mesh size is a good compromise between computing time and spatial resolution. Absolute tolerance is set at $A_{tol} = 10^{-8}$.

If the piston adheres to the surface of the phantom (Figure 5), computation time is approximately of 10 minutes on Intel Core2Quad Q6700 @ 2.67 GHz and 16Go of RAM to simulate 80 milliseconds of propagation. On the other hand, if piston is not adhering with phantom surface, computation time is approximately of 80 minutes. This problem, coming from the dynamical aspect of the resolution, is well-known and has been reported many times in the user community. The advice given by Comsol is imperfect.

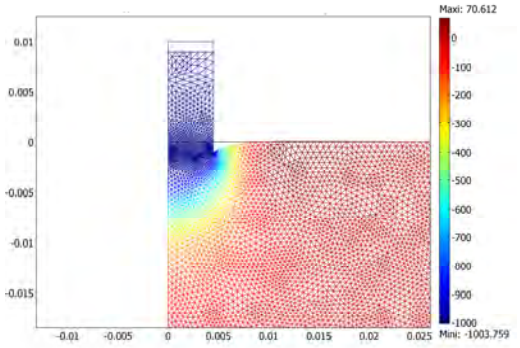


**Figure 5**. Longitudinal displacements in the 2D plane, induced by the piston at t = 7 ms. Colorbar is expressed in µm.

### 4.2. 3D model

In this section, we focused on a problem to take into account 3D objects in Comsol. Our objective was to implement a numerical 3D model for the liver, extracted from CT images, in its environment (heterogeneity, ribs, etc).

The anatomical model used comes from the IRCAD (Strasbourg, France). It contains the surface mesh of liver and ribs in *vtk* format (Figure 6). The import of this format in COMSOL is not an easy task without a CAD software from a third company.

Currently, we are interested in the propagation of shear wave generated by piston acting only on the liver. This liver has a volume of about 1.4 liters for a total of 400 984 tetrahedra (size <5 mm) and 1 742 796 degrees of freedom.

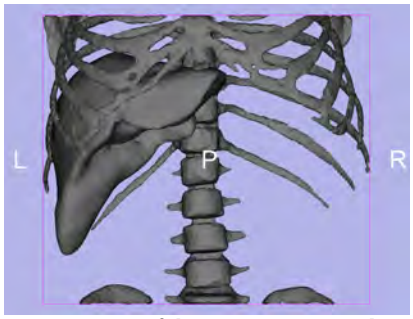


**Figure 6.** Geometry of the anatomy to consider

## 5. Results

### 5.1. 2D model of phantom

Simulation of shear wave propagation has validated the analytical and experimental measurements, in the good agreement with the expected Fibroscan®'s accuracy.
This comparison is reported, figures 7 to 9, for FEM, which reveals rebounds on lower fixed base (70 mm deep) which is due to the finite condition.

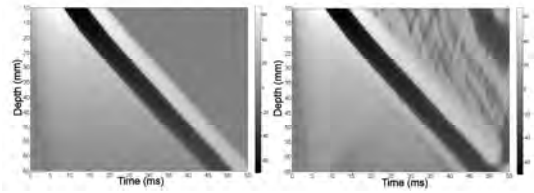


**Figure 7**. Comparison between analytical and simulated deformations in grayscale logarithmic.

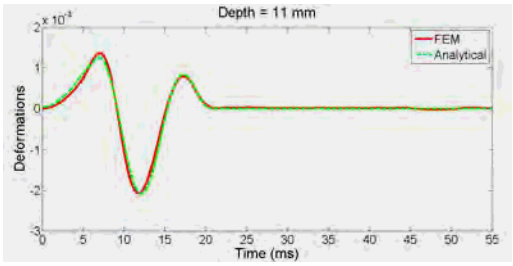


**Figure 8.** FEM and analytical results: deformation amplitudes at 11 mm of depth.

Figures 7-9 show that the shear wave propagates correctly in the mesh. We also verify on the amplitudes that the coupling effects are properly taken into account. The visible differences in the top-right of the right image of the figure 7 show the capability of FEM to solve propagation in a realistic bounded medium.

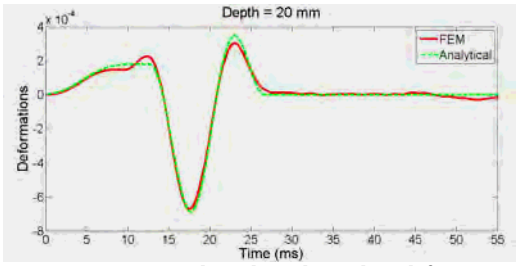


**Figure 9.** FEM and analytical results: deformation amplitudes at 20 mm of depth.

Figures 10 and 11 compare the deformations obtained by experiment and finite element simulation. Let us notice that, in the experimental case, it is difficult to properly respect the axi-symmetric geometry and the exact shape of the piston displacement.

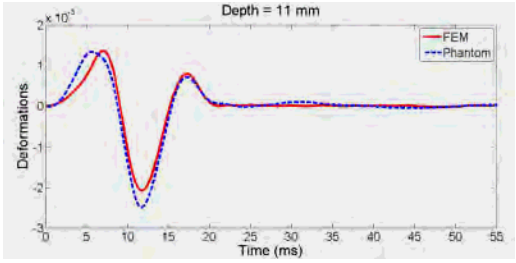


**Figure 10.** FEM and experimental results: deformation amplitudes at 11 mm of depth.

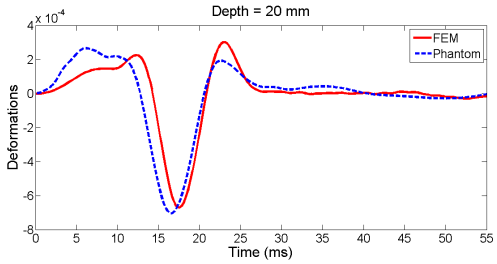


**Figure 11.** FEM and experimental results: deformation amplitudes at 20 mm of depth.

Noticeable differences are mainly due to the precision measurement of Young's modulus by Fibroscan®. At first, a small lag of 0.1 ms/cm appears between the two minima, corresponding to 0.17 kPa for the full range. That may be explained by the precision of Fibroscan®. Indeed, the value of Young's modulus chosen in the finite element model is provided by a measurement effected on the phantom. On the other hand, we observe on both figures 10 and 11 that the width of the impulse in the phantom increases with depth. That may be due to the weak viscosity of the phantom. It will be tested in the future, using viscoelastic Maxwell model.

### 5.2. Anatomical model

In 3D simulations, preliminary results are encouraging. Observations showed that the shear wave front is first spherical and then progressively deforms during propagation, according to the geometry of the liver.
Figure 12 shows the displacements for an *absolute* tolerance of only $10^{-5}$. Indeed, in this geometry, piston is not adhering with liver surface, therefore it is unfortunately impossible

to use the *absolute* tolerance of $10^{-8}$ that needs an unreachable time of computation (much more than 2 weeks).

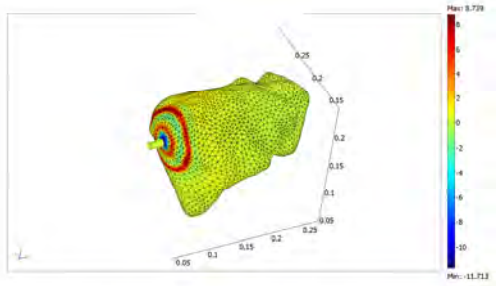

**Figure 12**. Example of displacement caused by a piston in the liver.

## 6. Conclusions

This study reveals promising results, regarding the feasibility to use FEM simulations, to understand the behavior of different tissue types and organs for Fibroscan® scanning. 3D simulations design will be improved using a complete thoracic and abdominal anatomy, to study potential sources of aberrant propagation patterns and velocity measures.

The results presented in this paper demonstrate the capabilities of a COMSOL Multiphysics to solve shear wave propagation in impulse elastography 2D problem.

This work initially focuses on solving problems in a uniform infinite half-space for which analytical solutions exist. After showing good agreement with these solutions, comparison with experimental data is available.

By including the measurement uncertainties, the shear wave arrival time and frequency content agree with experimental data.

Unfortunately, these results are not extrapolating on 3D model for a reasonable computation time.

## 7. References


1. J. Ophir, I. Cespedes, H. Ponnekanti, Y. Yazdi, and X. Li, Elastography: A quantitative method for imaging the elasticity of biological tissues, *Ultrasonic Imaging*, **13**, pp. 111-134, (1991).

2. L. Wei-Ning, C. M. Ingrassia, S. D. Fung-Kee-Fung, K. D. Costa, J. W. Holmes, and E. E. Konofagou, Theoretical Quality Assessment of Myocardial Elastography with In Vivo Validation, *Ultrasonics, Ferroelectrics and Frequency Control*, IEEE Transactions on, **54**, pp. 2233-2245, (2007).

3. C. L. de Korte, A. F. W. van der Steen, E. I. Céspedes, and G. Pasterkamp, Intravascular Ultrasound Elastography in Human Arteries: Initial Experience In Vitro, *Ultrasound in Medicine & Biology*, **24**, pp. 401-408, (1998).

4. R. Muthupillai, D. J. Lomas, P. J. Rossman, J. F. Greenleaf, A. Manduca, and R. L. Ehman, Magnetic resonance elastography by direct visualization of propagating acoustic strain waves, *Science*, **269**, pp. 1854-1857, (1995).

5. K. Hoyt, B. Castaneda, and K. J. Parker, Two-Dimensional Sonoelastographic Shear Velocity Imaging, *Ultrasound in Medicine & Biology*, **34**, pp. 276-288, (2008).

6. P. Sarvazyan, O. V. Rudenko, S. D. Swanson, J. B. Fowlkes, and S. Y. Emelianov, Shear wave elasticity imaging: a new ultrasonic technology of medical diagnostics, *Ultrasound in Medicine & Biology*, **24**, pp. 1419-1435, (1998).

7. L. Sandrin, M. Tanter, J. L. Gennisson, S. Catheline, and M. Fink, Shear elasticity probe for soft tissues with 1-D transient elastography, *Ultrasonics, Ferroelectrics and Frequency Control*, IEEE Transactions on, **49**, pp. 436-446, (2002).

8. K. Nightingale, M. S. Soo, R. Nightingale, and G. Trahey, Acoustic radiation force impulse imaging: in vivo demonstration of clinical feasibility, *Ultrasound in Medicine & Biology*, **28**, pp. 227-235, (2002)

9. L. Sandrin, B. Fourquet, J.-M. Hasquenoph, S. Yon, C. Fournier, F. Mal, C. Christidis, M. Ziol, B. Poulet, and F. Kazemi, Transient elastography: a new noninvasive method for assessment of hepatic fibrosis, *Ultrasound in Medicine & Biology*, **29**, pp. 1705-1713, (2003).

10. http://www.ircad.fr/softwares/3Dircadb/

11. K. Aki and P.G. Richards, Quantitative seismology, 2nd ed. ed. 2002, *Sausalito: University science books*. XVIII-700.

12. L. Sandrin, D. Cassereau, and M. Fink, The role of the coupling term in transient elastography, *J. Acoust. Soc. Am.* **115**, 73 (2004)